

## SUBARU HIGH-*z* EXPLORATION OF LOW-LUMINOSITY QUASARS (SHELLQs). I. DISCOVERY OF 15 QUASARS AND BRIGHT GALAXIES AT $5.7 < z < 6.9^{\dagger\dagger}$

YOSHIKI MATSUOKA<sup>1,2,3,\*</sup>, MASAFUSA ONOUE<sup>2</sup>, NOBUNARI KASHIKAWA<sup>1,2</sup>, KAZUSHI IWASAWA<sup>4</sup>, MICHAEL A. STRAUSS<sup>3</sup>, TOHRU NAGAO<sup>5</sup>, MASATOSHI IMANISHI<sup>1,2,6</sup>, MANA NIIDA<sup>7</sup>, YOSHIKI TOBA<sup>5</sup>, MASAYUKI AKIYAMA<sup>8</sup>, NAOKO ASAMI<sup>9</sup>, JAMES BOSCH<sup>3</sup>, SÉBASTIEN FOUCAUD<sup>10</sup>, HISANORI FURUSAWA<sup>1</sup>, TOMOTSUGU GOTO<sup>11</sup>, JAMES E. GUNN<sup>3</sup>, YUICHI HARIKANE<sup>12,13</sup>, HIROYUKI IKEDA<sup>1</sup>, TOSHIHIRO KAWAGUCHI<sup>14</sup>, SATOSHI KIKUTA<sup>2</sup>, YUTAKA KOMIYAMA<sup>1,2</sup>, ROBERT H. LUPTON<sup>3</sup>, TAKEO MINEZAKI<sup>15</sup>, SATOSHI MIYAZAKI<sup>1,2</sup>, TOMOKI MOROKUMA<sup>15</sup>, HITOSHI MURAYAMA<sup>16</sup>, ATSUSHI J. NISHIZAWA<sup>17</sup>, YOSHIAKI ONO<sup>12</sup>, MASAMI OUCHI<sup>12,16</sup>, PAUL A. PRICE<sup>3</sup>, HIROAKI SAMESHIMA<sup>18</sup>, JOHN D. SILVERMAN<sup>16</sup>, NAOSHI SUGIYAMA<sup>16,19</sup>, PHILIP J. TAIT<sup>6</sup>, MASAHIRO TAKADA<sup>16</sup>, TADAFUMI TAKATA<sup>1,2</sup>, MASAYUKI TANAKA<sup>1,2</sup>, JI-JIA TANG<sup>20</sup>, YOUSUKE UTSUMI<sup>21</sup>

*Submitted to The Astrophysical Journal*

### ABSTRACT

We report the discovery of 15 quasars and bright galaxies at  $5.7 < z < 6.9$ . This is the initial result from the Subaru High-*z* Exploration of Low-Luminosity Quasars (SHELLQs) project, which exploits the exquisite multi-band imaging data produced by the Subaru Hyper Suprime-Cam (HSC) Strategic Program survey. The candidate selection is performed by combining several photometric approaches including a Bayesian probabilistic algorithm to reject stars and dwarfs. The spectroscopic identification was carried out with the Gran Telescopio Canarias and the Subaru Telescope for the first 80 deg<sup>2</sup> of the survey footprint. The success rate of our photometric selection is quite high, approaching 100 % at the brighter magnitudes ( $z_{\text{AB}} < 23.5$  mag). Our selection also recovered all the known high-*z* quasars on the HSC images. Among the 15 discovered objects, six are likely quasars, while the other six with interstellar absorption lines and in some cases narrow emission lines are likely bright Lyman-break galaxies. The remaining three objects have weak continua and very strong and narrow Ly  $\alpha$  lines, which may be excited by ultraviolet light from both young stars and quasars. These results indicate that we are starting to see the steep rise of the luminosity function of  $z \geq 6$  galaxies, compared to that of quasars, at magnitudes fainter than  $M_{1450} \sim -22$  mag or  $z_{\text{AB}} \sim 24$  mag. Follow-up studies of the discovered objects as well as further survey observations are ongoing.

*Subject headings:* dark ages, reionization, first stars — galaxies: active — galaxies: high-redshift — intergalactic medium — quasars: general — quasars: supermassive black holes

### 1. INTRODUCTION

The era from the birth of the first stars to cosmic reionization is one of the key subjects in astronomy and astrophysics today. While the formation of the first stars is still largely unexplored observationally, the epoch of reionization is being explored with several different approaches. The latest measurements of the cosmic microwave background (CMB) by the *Planck* space mission suggest a reionization optical depth of  $\tau = 0.066 \pm 0.016$ . When interpreted as a sharp transition from a neutral to ionized intergalactic medium (IGM), this corresponds to a reionization redshift of  $z = 8.8_{-1.4}^{+1.7}$  (Planck Collaboration 2015). This value is marginally consistent with the rapid decline of the

<sup>18</sup> Koyama Astronomical Observatory, Kyoto-Sangyo University, Kita, Kyoto, 603-8555, Japan.

<sup>19</sup> Graduate School of Science, Nagoya University, Furo-cho, Chikusa-ku, Nagoya 464-8602, Japan.

<sup>20</sup> Institute of Astronomy and Astrophysics, Academia Sinica, Taipei, 10617, Taiwan.

<sup>21</sup> Hiroshima Astrophysical Science Center, Hiroshima University, Higashi-Hiroshima, Hiroshima 739-8526, Japan.

\* E-mail: yk.matsuoka@nao.ac.jp.

<sup>†</sup> Based on data collected at the Subaru Telescope, which is operated by the National Astronomical Observatory of Japan.

<sup>‡</sup> Based on observations made with the Gran Telescopio Canarias (GTC), installed at the Spanish Observatorio del Roque de los Muchachos of the Instituto de Astrofísica de Canarias, on the island of La Palma.

<sup>1</sup> National Astronomical Observatory of Japan, Mitaka, Tokyo 181-8588, Japan.

<sup>2</sup> Department of Astronomy, School of Science, Graduate University for Advanced Studies, Mitaka, Tokyo 181-8588, Japan.

<sup>3</sup> Princeton University Observatory, Peyton Hall, Princeton, NJ 08544, USA.

<sup>4</sup> ICREA and Institut de Ciències del Cosmos, Universitat de Barcelona, IEEC-UB, Martí i Franquès, 1, 08028 Barcelona, Spain.

<sup>5</sup> Research Center for Space and Cosmic Evolution, Ehime University, Matsuyama, Ehime 790-8577, Japan.

<sup>6</sup> Subaru Telescope, Hilo, HI 96720, USA.

<sup>7</sup> Graduate School of Science and Engineering, Ehime University, Matsuyama, Ehime 790-8577, Japan.

<sup>8</sup> Astronomical Institute, Tohoku University, Aoba, Sendai, 980-8578, Japan.

<sup>9</sup> Japan Professional School of Education, Chiyoda, Tokyo 101-0041, Japan.

<sup>10</sup> Department of Physics and Astronomy, Shanghai JiaoTong University, Shanghai 200240, China.

<sup>11</sup> Institute of Astronomy and Department of Physics, National Tsing Hua University, Hsinchu 30013, Taiwan.

<sup>12</sup> Institute for Cosmic Ray Research, The University of Tokyo, Kashiwa, Chiba 277-8582, Japan

<sup>13</sup> Department of Physics, Graduate School of Science, The University of Tokyo, Bunkyo, Tokyo 113-0033, Japan

<sup>14</sup> Department of Liberal Arts and Sciences, Sapporo Medical University, Chuo, Sapporo 060-8556, Japan.

<sup>15</sup> Institute of Astronomy, The University of Tokyo, Mitaka, Tokyo 181-0015, Japan.

<sup>16</sup> Kavli Institute for the Physics and Mathematics of the Universe, WPI, The University of Tokyo, Kashiwa, Chiba 277-8583, Japan.

<sup>17</sup> Institute for Advanced Research, Nagoya University, Furo-cho, Chikusa-ku, Nagoya 464-8602, Japan.

H I neutral fraction from  $z \sim 8$  to  $z \sim 6$ , inferred from the evolving Ly  $\alpha$  luminosity function of galaxies (e.g., Ouchi et al. 2008, 2010; Konno et al. 2014; Bouwens et al. 2015; Choudhury et al. 2015). At  $z \sim 6$ , the Universe is in the final phase of reionization, as indicated by the small H I optical depth of the IGM estimated from the Gunn & Peterson (1965, GP hereafter) troughs of luminous high- $z$  quasars (Fan et al. 2006a).

The main source of the ultraviolet (UV) photons that caused the reionization of the Universe is still under debate. It has been argued that star-forming galaxies observed in deep surveys are not able to produce sufficient number of photons to sustain reionization (e.g., Robertson et al. 2010, 2013), while the revised *Planck* results may alleviate this problem (Robertson et al. 2015). Active galactic nuclei (AGNs) have been studied as a possible additional source of ionizing photons (e.g., Lehnert & Bremer 2003; Fontanot et al. 2012; Grissom et al. 2014; Giallongo et al. 2015; Madau & Haardt 2015), but the results are still controversial, largely due to the lack of knowledge about the numbers of faint AGNs residing in the reionization era.

High- $z$  quasars are a key population to understand the formation and evolution of supermassive black holes (SMBHs) as well. If the assembly of a SMBH is predominantly via gas accretion onto a seed black hole with mass  $M_{\text{BH},0}$ , then the time needed to grow to the mass  $M_{\text{BH}}$  is

$$\begin{aligned} t &= t_{\text{Edd}} \left( \frac{\epsilon}{1-\epsilon} \right) \lambda_{\text{Edd}}^{-1} \ln \left( \frac{M_{\text{BH}}}{M_{\text{BH},0}} \right) \\ &= 0.043 \ln \left( \frac{M_{\text{BH}}}{M_{\text{BH},0}} \right) \text{ Gyr}, \end{aligned}$$

where  $t_{\text{Edd}} = 0.44 \mu_e^{-1} \text{ Gyr}$  is the Eddington timescale,  $\mu_e$  is the mean molecular weight per electron,  $\epsilon$  is the radiative efficiency, and  $\lambda_{\text{Edd}}$  is the Eddington ratio (Shapiro 2005; Madau et al. 2014); here we assume that  $\lambda_{\text{Edd}}$  is constant in time. We adopt  $\mu_e = 1.15$ ,  $\epsilon = 0.1$ , and  $\lambda_{\text{Edd}} = 1.0$  to derive the second line of the equation. For example, a seed with  $M_{\text{BH},0} = 100 M_{\odot}$  will take 0.7 Gyr to form a quasar with  $M_{\text{BH}} = 10^9 M_{\odot}$ . Since this timescale is comparable to the cosmic time elapsed between  $z = 20$  and  $z = 6$ , the SMBH mass functions at  $z > 6$  convey critical information about the mass distribution of the seed black holes and the mode of subsequent growth, including super-Eddington accretion (Kawaguchi et al. 2004). Indeed, recent discoveries of the luminous quasars ULAS J1120+0641 with  $M_{\text{BH}} \sim 2 \times 10^9 M_{\odot}$  at  $z = 7.085$  (Mortlock et al. 2011) and SDSS J0100+2802 with  $M_{\text{BH}} \sim 1 \times 10^{10} M_{\odot}$  at  $z = 6.30$  (Wu et al. 2015) have made a significant impact on such models (e.g., Volonteri 2012; Ferrara et al. 2014; Madau et al. 2014).

Furthermore, high- $z$  quasars are a signpost of galaxies and high density peaks in the dark matter distribution in the early Universe. The stellar and gaseous properties in and around the host galaxies can be studied in the optical/infrared (e.g., Kashikawa et al. 2007; Goto et al. 2009, 2012; Willott et al. 2011) or at sub-mm/radio wavelengths (e.g., Maiolino et al. 2005; Wang et al. 2007; Venemans et al. 2012, 2016; Wang et al. 2013; Willott et al. 2013, 2015), giving a unique probe of galax-

ies in the reionization era. The chemical enrichment, and thus the preceding star formation history, can be measured with strong metal emission lines arising from ionized gas around the quasar nuclei (e.g., Jiang et al. 2007; De Rosa et al. 2011, 2014). On the whole, no or little chemical evolution of quasars has been observed from  $z \sim 7$  to the local Universe. A good example of this is ULAS J1120+0641, whose emission-line and continuum spectrum is strikingly similar to those of the local quasars except for the deep GP trough.

In the last two decades, there has been great progress in the quest for high- $z$  quasars<sup>25</sup>. The SDSS (York et al. 2000) provided the first opportunity to search for high- $z$  quasars over wide fields ( $> 1000 \text{ deg}^2$ ), resulting in several tens of objects published to date (Fan et al. 2000, 2001a, 2003, 2004, 2006b; Jiang et al. 2008, 2009, 2015). The Canada-France High- $z$  Quasar Survey (CFHQS; Willott et al. 2005, 2007, 2009, 2010a,b) explored fainter magnitudes than the SDSS and found a few tens of new quasars, including one very faint object (CFHQS J0216–0455;  $z_{\text{AB}} = 24.4 \text{ mag}$  at  $z = 6.01$ ) discovered in the Subaru XMM-Newton Deep Survey (SXDS; Furusawa et al. 2008) area. However, these optical surveys are not sensitive to redshifts beyond  $z = 6.5$ , where quasars become almost invisible at observed wavelengths  $\lambda_{\text{obs}} < 0.9 \mu\text{m}$  due to strong IGM absorption. The first quasar discovered at  $z > 6.5$  is ULAS J1120+0641 mentioned above, which was selected from near-infrared (NIR) data of the United Kingdom Infrared Telescope (UKIRT) Infrared Deep Sky Survey (UKIDSS; Lawrence et al. 2007). With the advent of the Visible and Infrared Survey Telescope for Astronomy (VISTA) Kilo-degree Infrared Galaxy (VIKING) survey, more  $z > 6.5$  quasars are being discovered (Venemans et al. 2013, 2015b). New optical wide-field surveys such as the Panoramic Survey Telescope & Rapid Response System 1 (Pan-STARRS1; Kaiser et al. 2010)  $3\pi$  survey and the Dark Energy Survey (Dark Energy Survey Collaboration 2016) are equipped with a  $y$ -band filter centered at  $9500 - 10000 \text{ \AA}$ , and are starting to deliver many more quasars at  $6 \leq z \leq 7$  (Bañados et al. 2014; Reed et al. 2015). In addition, there are various smaller projects which have succeeded in identifying high- $z$  quasars (e.g., Goto 2006; Carnall et al. 2015; Kashikawa et al. 2015; Kim et al. 2015). In total, the above surveys have identified about a hundred high- $z$  quasars published to date. Most of the quasars are located at  $z < 6.5$  and  $z_{\text{AB}} < 22.5 \text{ mag}$ , while the higher redshifts and fainter magnitudes are still poorly explored. The known bright high- $z$  quasars must be just the tip of the iceberg predominantly comprised of faint quasars and AGNs, which may be a significant contributor to reionization, and may represent the more typical mode of SMBH growth in the early Universe.

This paper describes our ongoing project, SHEL-LQs (Subaru High- $z$  Exploration of Low-Luminosity Quasars), which is the first  $1,000\text{-deg}^2$  class survey for high- $z$  quasars with a 8-m class telescope. The project exploits multi-band photometry data produced by the Subaru Hyper Suprime-Cam (HSC) Subaru Strategic

<sup>25</sup> Hereafter, “high- $z$ ” denotes  $z > 5.7$ , where quasars are observed as  $i$ -band dropouts in the Sloan Digital Sky Survey (SDSS) filter system (Fukugita et al. 1996).

Program (SSP) survey. We present the results of the initial follow-up spectroscopy of photometric candidates, performed in the 2015 Fall and 2016 Spring semesters, which delivered 15 high- $z$  objects including both quasars and bright galaxies. This paper is organized as follows. We introduce the Subaru HSC-SSP survey in §2. The details of the photometric candidate selection are presented in §3. The spectroscopic follow-up observations are described in §4. The quasars and galaxies we have discovered are presented and discussed in §5. The summary appears in §6. We adopt the cosmological parameters  $H_0 = 70 \text{ km s}^{-1} \text{ Mpc}^{-1}$ ,  $\Omega_M = 0.3$ , and  $\Omega_\Lambda = 0.7$ . All magnitudes in the optical and NIR bands are presented in the AB system (Oke & Gunn 1983). Magnitudes refer to point spread function (PSF) magnitudes (see §2) corrected for Galactic extinction (Schlegel et al. 1998) unless otherwise noted.

## 2. THE SUBARU HSC-SSP SURVEY

The Subaru HSC-SSP survey (Takada et al., in prep.) is a large collaborative project contributed by researchers in Japan, Taiwan, and Princeton University. The project started in early 2014, and will include 300 nights, ending in 2019. It uses the HSC (Miyazaki et al. 2012, Miyazaki et al., in prep.), a wide-field camera newly installed on the Subaru 8.2-m telescope on the summit of Maunakea. HSC is equipped with 116  $2\text{K} \times 4\text{K}$  Hamamatsu fully-depleted CCDs, of which 104 CCDs are used to obtain science data. The pixel scale is  $0''.17$ . The camera has a nearly circular field-of-view of  $1^\circ.5$  diameter, which enables it to image  $1.77 \text{ deg}^2$  of the sky in a single shot. Five broad-band filters ( $g$ ,  $r$ ,  $i$ ,  $z$ , and  $y$ ) and several narrow-band filters are currently available.

The HSC-SSP survey has three layers with different combinations of area and depth. The Wide layer aims to observe  $1,400 \text{ deg}^2$  mostly along the celestial equator through the five broad-band filters. The present paper is based on this Wide layer data. The total exposure times range from 10 min in the  $g$ ,  $r$  bands to 20 min in the  $i$ ,  $z$ , and  $y$  bands, divided into individual exposures of  $\sim 3$  min each. The target  $5\sigma$  limiting magnitudes are ( $g$ ,  $r$ ,  $i$ ,  $z$ ,  $y$ ) = (26.5, 26.1, 25.9, 25.1, 24.4) mag measured in  $2''.0$  aperture. The Deep and Ultra-Deep layers observe  $27$  and  $3.5 \text{ deg}^2$ , respectively, within and around popular deep survey fields. Five broad-band filters and four narrow-band filters are used, aiming to reach the  $5\sigma$  limiting depth of  $r = 27.1$  mag (Deep) or  $r = 27.7$  mag (Ultra-Deep).

The SHELLQs project exploits the exquisite HSC survey data to search for low-luminosity quasars at high redshift. Assuming the quasar luminosity function at  $z \geq 6$  presented by Willott et al. (2010b), the expected numbers of newly identified quasars in the Wide layer are  $\sim 500$  with  $z_{\text{AB}} < 24.5$  mag at  $z \sim 6$  and  $\sim 100$  with  $z_{\text{AB}} < 24.0$  mag at  $z \sim 7$ . The former magnitude limit corresponds to  $M_{1450} < -22$  mag for a typical quasar spectral energy distribution (SED), thus allowing us to explore  $\sim 2$  mag lower luminosity than any previous wide-field survey at  $z \sim 6$  (e.g., Jiang et al. 2009). Our filter set is sensitive to quasars with redshifts up to  $z \sim 7.4$ , i.e., beyond the current quasar redshift record. However, the detection capability sharply drops at  $z > 7$  where the GP trough comes into the  $y$  band, hence the survey is limited to intrinsically very luminous objects at those

redshift. The deep optical data produced by the HSC survey will also provide opportunities to explore even higher redshifts when combined with wide and deep NIR surveys.

This paper describes the results from the early HSC survey data taken before 2015 August. It covers roughly  $80 \text{ deg}^2$  in the five broad bands in the Wide layer, with the median seeing of  $0''.6 - 0''.8$ . Data reduction was performed with the dedicated pipeline `hscPipe` (version 3.8.5; Bosch et al., in prep.) derived from the Large Synoptic Survey Telescope software pipeline<sup>26</sup> (Jurić et al. 2015), for all the standard procedures including bias subtraction, flat fielding with dome flats, stacking, astrometric and photometric calibrations, as well as source detection and measurements. The astrometric and photometric calibrations are tied to the Pan-STARRS1 system<sup>27</sup> (Schlafly et al. 2012; Tonry et al. 2012; Magnier et al. 2013). We utilize forced photometry, which allows for flux measurements in all the five bands with a consistent aperture defined in a reference band. The reference band is  $i$  by default and is switched to  $z$  ( $y$ ) for extremely red sources with no detection in the  $i$  ( $z$ ) and bluer bands. We use the PSF magnitude ( $m_{\text{PSF}}$ , or simply  $m$ ) and the cModel magnitude ( $m_{\text{cModel}}$ ), which are measured by fitting the PSF models and two-component, PFS-convolved galaxy models to the source profile, respectively (Abazajian et al. 2004). We measure fluxes and colors of sources with  $m_{\text{PSF}}$ , while the source extendedness is evaluated with  $m_{\text{PSF}} - m_{\text{cModel}}$ .

We performed a rough assessment of the completeness limits achieved in the early Wide survey as follows. In each subregion of the sky with approximate size of  $12' \times 12'$ , we select all the sources whose processing flags indicate clean photometry, and measure the number counts  $N(m)$ . It typically follows a straight line in the  $m - \log[N(m)]$  plane at bright magnitudes, then peaks at  $m = m_{\text{peak}}$ . We fit a straight line  $\tilde{N}(m)$  to the  $m - \log[N(m)]$  relation at  $m_{\text{peak}} - 5 < m < m_{\text{peak}} - 1$  and define the 50 % completeness magnitude at the point where  $N(m)$  falls to one-half of  $\tilde{N}(m)$ . The resultant completeness magnitudes averaged over all the fields are (26.5, 26.3, 26.4, 25.5, 24.7) mag in the ( $g$ ,  $r$ ,  $i$ ,  $z$ ,  $y$ ) band, respectively, with a typical field-to-field variation of 0.3 mag. The spatial pattern of the above estimates agrees with that of the seeing, in such a way that poor seeing is

<sup>26</sup> This paper makes use of software developed for the Large Synoptic Survey Telescope (LSST). We thank the LSST Project for making their code available as free software at <http://dm.lsstcorp.org>.

<sup>27</sup> The Pan-STARRS1 Surveys (PS1) have been made possible through contributions of the Institute for Astronomy, the University of Hawaii, the Pan-STARRS Project Office, the Max-Planck Society and its participating institutes, the Max Planck Institute for Astronomy, Heidelberg and the Max Planck Institute for Extraterrestrial Physics, Garching, The Johns Hopkins University, Durham University, the University of Edinburgh, Queen's University Belfast, the Harvard-Smithsonian Center for Astrophysics, the Las Cumbres Observatory Global Telescope Network Incorporated, the National Central University of Taiwan, the Space Telescope Science Institute, the National Aeronautics and Space Administration under Grant No. NNX08AR22G issued through the Planetary Science Division of the NASA Science Mission Directorate, the National Science Foundation under Grant No. AST-1238877, the University of Maryland, Eotvos Lorand University (ELTE) and the Los Alamos National Laboratory.

accompanied by worse-than-average depth. These completeness magnitudes are roughly 0.3 mag fainter than the target limiting magnitudes of the survey mentioned above, which is at least partly because of the differences in the adopted magnitudes (PSF magnitudes or  $2''.0$ -aperture magnitudes) and in the definitions of the depths (50-% completeness or  $5\sigma$  detection).

Our project benefits from archival NIR data from UKIDSS and VIKING. The UKIDSS is a multi-tiered imaging survey using WFCAM, a wide field camera mounted on the UKIRT 3.8-m telescope (Lawrence et al. 2007). The widest Large Area Survey covers most of the HSC survey footprint, with the target  $5\sigma$  limiting magnitudes of  $(Y, J, H, K) = (20.9, 20.4, 20.0, 20.1)$  mag measured in  $2''.0$  aperture. The VIKING is one of the public surveys of the European Southern Observatory with the VISTA 4.1-m telescope. This project aims to observe  $1,500 \text{ deg}^2$  of the sky, with the target  $5\sigma$  limiting magnitudes of  $(Z, Y, J, H, K) = (23.1, 22.3, 22.1, 21.5, 21.2)$  mag measured in  $2''.0$  aperture. Roughly half of the HSC survey footprint will be covered by the VIKING at its completion.

### 3. PHOTOMETRIC CANDIDATE SELECTION

High- $z$  quasars are characterized by extremely red optical colors caused by strong IGM absorption bluewards of Ly  $\alpha$ . This is demonstrated in Figure 1, which presents  $i-z$  and  $z-y$  colors of model quasars and other populations in the HSC passband system. There are two major sources of astrophysical contamination to the photometric selection of quasars. One is Galactic brown dwarfs, which have been the most serious contaminants in past surveys because of their very red colors and point-like appearance. The other is faint Lyman break galaxies (LBGs) at  $z \geq 6$ , which are also affected by IGM absorption. We expect that the excellent image quality of the HSC will help distinguish quasars and galaxies morphologically, but this remains to be confirmed. Figure 2 displays the luminosity functions of high- $z$  quasars (Willott et al. 2010b) and LBGs (Bouwens et al. 2006, 2011). Although they are still poorly constrained at  $M_{1450} > -24$  mag for quasars and at  $M_{1350} < -22$  for LBGs, it is likely that the two functions intersect at apparent magnitude of  $\sim 24$  mag, with LBGs outnumbering quasars at fainter magnitudes. This is why previous surveys at brighter magnitudes did not suffer from severe LBG contamination. Note also that the usual assumption that high- $z$  quasars are point sources may not be valid for low-luminosity populations due to the host galaxy contribution.

There are several methods to extract quasar candidates from multi-band imaging data. Our Main sample of candidates is selected based on a Bayesian probabilistic approach, as detailed in §3.1. It computes the posterior probability for each source being a high- $z$  quasar rather than a red star or dwarf, based on photometry in all the available bands as well as SED and surface density models of the populations under consideration. We use photometry in the HSC optical bands plus the NIR bands  $(Y, J, H, K)$  where available from UKIDSS or VIKING. In addition, we construct an Auxiliary sample of candidates with two approaches, namely, classical SED fitting and simple color cuts, as described in §3.2. These additional selections allow us to evaluate possible bias and

incompleteness inherent to the Bayesian approach and thus complement the Main sample. We describe the entire flow of the candidate selection from the HSC-SSP database to the final spectroscopic targets in §3.3. Our selection procedure has efficiently removed contaminants, recovered all the known quasars imaged by the HSC so far (§3.4), and discovered a number of new objects as described in the following sections.

#### 3.1. Main sample

The Main sample of quasar candidates is selected with a Bayesian probabilistic algorithm, developed following Mortlock et al. (2012). Here we assume that galaxies and relatively blue stars with O to early-M spectral types have been removed in advance with color and extendedness cuts (see §3.3), and we therefore do not model a population of LBGs. For a detected source with the observed quantities  $\vec{d}$ , the Bayesian probability  $P_Q^B$  of being a quasar is given by:

$$P_Q^B(\vec{d}) = \frac{W_Q(\vec{d})}{W_Q(\vec{d}) + W_D(\vec{d})} \quad (1)$$

and

$$W_{Q/D}(\vec{d}) = \int S(\vec{p}) Pr(\text{det}|\vec{p}) Pr(\vec{d}|\vec{p}) d\vec{p} \quad (2)$$

where the subscripts Q and D denote a quasar and a brown dwarf, respectively. The vector  $\vec{d}$  represents the magnitudes in all the available bands in the present case, while  $\vec{p}$  represents the intrinsic source properties, i.e., luminosity and redshift for a quasar and luminosity and spectral type for a brown dwarf. The functions  $S(\vec{p})$ ,  $Pr(\text{det}|\vec{p})$ , and  $Pr(\vec{d}|\vec{p})$  represent the surface number density, the probability that the source is detected (“det”), and the probability that the source has the observed quantities  $\vec{d}$ , respectively, each as a function of  $\vec{p}$ .

We compute  $S(\vec{p})$  with the quasar luminosity function of Willott et al. (2010b) and the Galactic brown dwarf model of Caballero et al. (2008). The latter model takes into account the spatial density distributions and luminosities of late-M, L, and T dwarfs and allows one to compute number counts for each spectral type at a given Galactic coordinate. Since the HSC-SSP survey depth has not been fully analyzed yet (§2), we arbitrarily set  $Pr(\text{det}|\vec{p}) = 1$  for  $z_{\text{AB}} < 26.0$  or  $y_{\text{AB}} < 25.0$  mag and 0 otherwise. The SED models required for  $Pr(\vec{d}|\vec{p})$  are created as follows. The quasar model spectrum at  $z = 0$  is first created by stacking the SDSS spectra of 340 bright quasars at  $z \simeq 3$ , where the quasar selection is fairly complete (Richards et al. 2002; Willott et al. 2005), after correcting for the foreground IGM absorption. The IGM H I opacity data are taken from Songaila (2004). This spectrum is then placed at various redshifts with the appropriate IGM absorption taken into account, and convolved with the filter transmission functions to compute colors. Since the model spectra redshifted to  $z > 6$  do not extend beyond the  $J$  band, we take the  $J-H$  and  $H-K$  colors from Hewett et al. (2006). The dwarf colors are computed with a set of observed spectra compiled

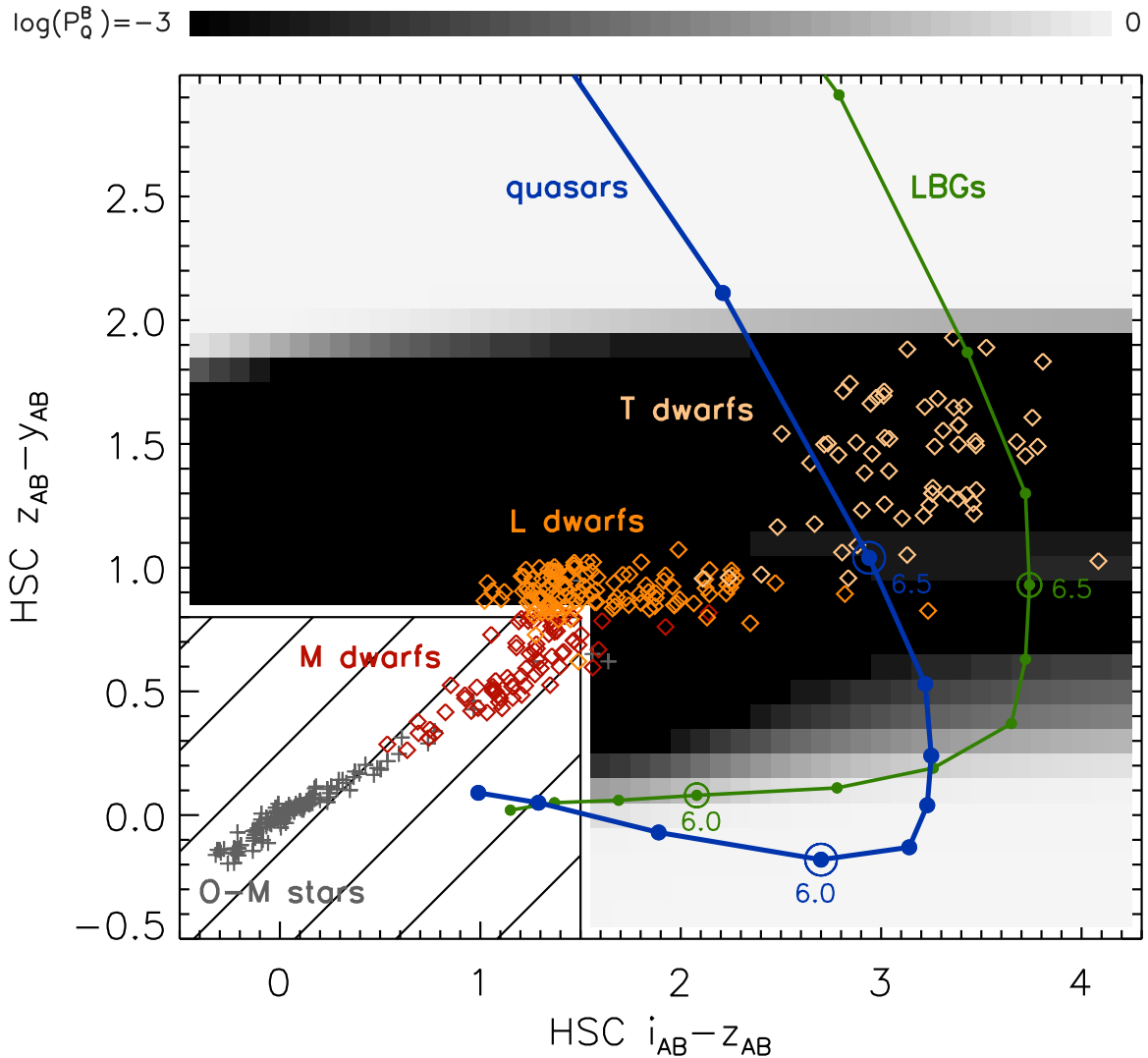


FIG. 1.— The  $i - z$  and  $z - y$  colors of high- $z$  quasars (blue line) and galaxies (green line), as well as Galactic stars and brown dwarfs (crosses and diamonds). The SED models for quasars and brown dwarfs are described in §3.1. The galaxy colors are calculated with the spectral templates taken from González et al. (2012), while the colors of O – M stars are computed with the Pickles (1998) library. The dots along the blue and green lines represent redshifts in steps of 0.1, with  $z = 6.0$  and  $6.5$  marked by the large open circles. The hatched area in lower left indicates the color space excluded from the HSC-SSP database query in the first step of our quasar selection (§3.3). As a demonstration, the grey scale represents the Bayesian quasar probabilities  $P_Q^B$  (Equations 1 and 2; the color bar is found at the top) over this plane, assuming  $z_{AB} = 24.0$  mag and the  $5\sigma$  limiting magnitudes of  $(i_{AB}, z_{AB}, y_{AB}) = (26.5, 25.5, 25.0)$  mag. Galaxy models are not included in the Bayesian algorithm at present.

in the SpeX prism library<sup>28</sup> and in the CGS4 library<sup>29</sup>. Because of the discrete sampling of the brown-dwarf templates grouped into individual spectral types, the integration in Equation 2 is treated as a summation for spectral types. Finally, the flux errors are taken from the outputs of the HSC image processing pipeline, and are assumed to follow a Gaussian probability density distribution in the flux unit.

### 3.2. Auxiliary sample

While the Bayesian algorithm is quite efficient in eliminating contaminants, it may be subject to unknown bias

<sup>28</sup> This research has benefitted from the SpeX Prism Spectral Libraries, maintained by Adam Burgasser at <http://pono.ucsd.edu/~adam/browndwarfs/spexprism>.

<sup>29</sup> The L and T dwarf archive maintained by Sandy Leggett at <http://staff.gemini.edu/~sleggett/LTdata.html>.

or incompleteness because of its dependence on empirical SED and surface density models. In order to monitor these effects and complement the Main sample, we create an Auxiliary sample of candidates with two independent methods, i.e., classical SED fitting and simple color cuts. As in the Main selection, galaxies and relatively blue stars are assumed to be removed before the following selections are performed.

The SED fitting algorithm fits a wide variety of spectral models to the observed fluxes in all the available HSC, UKIDSS, and VIKING bands. Each quasar model is a combination of power-law continuum and emission lines with a Gaussian profile, assuming various values of power-law slope, line strength, and dust extinction, drawn from the statistics measured at  $z > 3$  (Fan et al. 2001b; Diamond-Stanic et al. 2009). We use the dust extinction law for the Small Magellanic Cloud (Prevot et al. 1984). The models of stars and brown

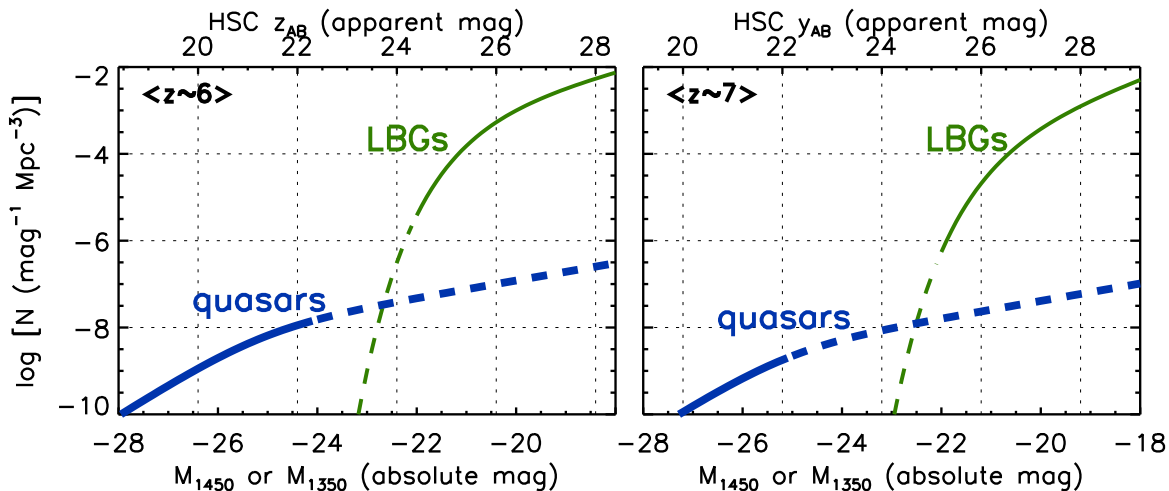


FIG. 2.— Luminosity functions of quasars (thick blue lines, as a function of  $M_{1450}$ ; Willott et al. 2010b) and LBGs (thin green lines, as a function of  $M_{1350}$ ; Bouwens et al. 2006, 2011) at  $z \sim 6$  (left) and  $z \sim 7$  (right). The corresponding apparent magnitudes for quasars in the HSC  $z$  or  $y$  band are indicated on the upper axis. Although the luminosity functions are poorly constrained in the ranges marked by the dashed lines, LBGs likely outnumber quasars at apparent magnitudes fainter than  $\sim 24$  mag.

dwarfs are taken from the Kurucz (1993) and Allard (2012) libraries assuming solar metallicity. The fitting is performed with the standard  $\chi^2$  minimization method using the photometric errors from the pipeline, and assigns a quasar probability  $P_Q^S$  to each candidate, with no Bayesian prior (i.e., no weighting by the  $S(\vec{p})$  from Equation 2).

We also consider the following simple color cuts for the candidate selection:

$$(i_{\text{PSF}} - z_{\text{PSF}} > 2.0 \text{ and } z_{\text{PSF}} - y_{\text{PSF}} < 0.5) \\ \text{or} \\ (z_{\text{PSF}} - y_{\text{PSF}} > 2.0).$$

The above criteria are based on the quasar locus on the  $i - z$  versus  $z - y$  diagram shown in Figure 1. Each candidate is assigned  $P_Q^C = 1$  if it satisfies the color criteria and 0 otherwise. The magnitude limits are described in the next section.

### 3.3. Selection flow

The present work is based on the HSC-SSP Wide-layer data included in the S15A internal data release, which happened in 2015 September. Forced photometry (see §2) on the stacked images is used. We first query the HSC-SSP database for non-blended<sup>30</sup> sources meeting the following criteria:

$$(z_{\text{AB}} < 24.5 \text{ and } \sigma_z < 0.155 \text{ and } i_{\text{AB}} - z_{\text{AB}} > 1.5 \\ \text{and } z_{\text{AB}} - z_{\text{cModel,AB}} < 0.3) \quad (3)$$

or

$$(y_{\text{AB}} < 24.0 \text{ and } \sigma_y < 0.155 \text{ and } z_{\text{AB}} - y_{\text{AB}} > 0.8 \\ \text{and } y_{\text{AB}} - y_{\text{cModel,AB}} < 0.3) \quad (4)$$

and without any critical quality flags assigned.<sup>31</sup> Throughout this paper  $i_{\text{AB}}$ ,  $z_{\text{AB}}$ , and  $y_{\text{AB}}$  refer to PFS

<sup>30</sup> In particular, we query sources that are isolated or deblended from parent blended sources, and we reject those parents. This corresponds to `deblend.nchild = 0` in the database language.

<sup>31</sup> Specifically, we require that the source is (i) not close to an edge of the processed image frame (`flags.pixel.edge =`

magnitudes. The first two lines of conditions select  $i$ -band dropouts at  $z \sim 6$ , while the latter two select  $z$ -band dropouts at  $z \sim 7$ . The color cuts are used to exclude relatively blue stars with O to early-M spectral types (see Figure 1), while the difference between the PSF and cModel magnitudes is used to exclude extended sources. After the database query, we further remove low- $z$  interlopers with more than  $3\sigma$  detection in the  $g$  or  $r$  band.

The above initial candidates are matched to the UKIDSS and VIKING catalogs within  $1''.0$  in the overlapping survey area, and then processed through the Bayesian selection algorithm. Those with significant quasar probability,  $P_Q^B > 0.1$ , are added to the Main sample of candidates. Those with lower  $P_Q^B$  are further checked with the SED-fitting algorithm and the simple color-cut criteria described in §3.2, and added to the Auxiliary sample if  $P_Q^S > 0.1$  or  $P_Q^C = 1$ . We calculated  $P_Q^S$  and  $P_Q^C$  for the objects in the Main sample as well and found that they always meet the Auxiliary selection criteria, i.e., the Main sample is a subsample of the Auxiliary sample.

Because we are looking for rare faint objects detected in only one or two bands, we are sensitive to false dropout sources of both astrophysical and non-astrophysical origins, as described below. However, we can take advantage of the fact that in the HSC-SSP Wide survey, each patch of the sky is visited and imaged several times with different dithering positions. Glitches in the data may become apparent upon comparing the individual per-visit exposures. For every candidate, we retrieve and perform photometry on all the per-visit images with Source Extractor, version 2.8.6 (Bertin & Arnouts 1996), in the double-image mode, with the stacked image as the detection reference. If any of the per-visit photometric measurements deviate by more than three times the measure-

False), (ii) not in a bad CCD region (i.e., bad pixels or vignetting area; `flags.bad.center = False`), (iii) not saturated (`flags.pixel.saturated.center = False`), and (iv) not affected by cosmic rays (`flags.pixel.cr.center = False`), in the  $i$ ,  $z$ , and  $y$  bands.



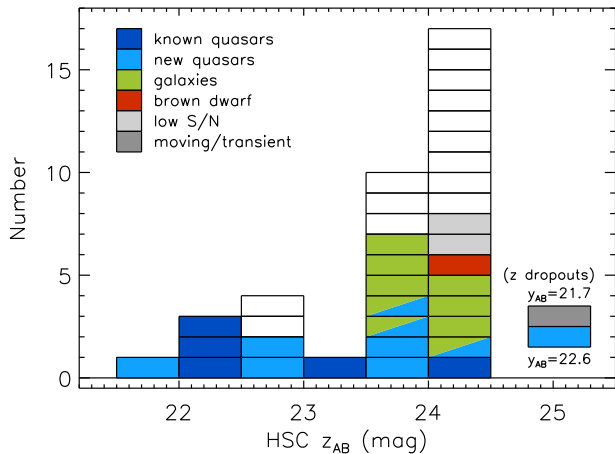


FIG. 3.— Magnitude histogram of the 38 Main candidates. The five dark blue cells represent high- $z$  quasars known prior to our survey. The remaining cells are color-coded according to the results of our follow-up spectroscopy (see §4) as follows. Light blue: high- $z$  quasars, green: high- $z$  galaxies, red: brown dwarf, dark grey: moving object or transient event, light grey: ambiguous nature due to the low spectral S/N, white: awaiting spectroscopy. The two cells in lower right represent  $z$ -band dropouts. The success rate of our photometric quasar selection is quite high, approaching 100 % at the brighter magnitudes ( $z_{AB} < 23.5$  mag). Most of the contaminants at fainter magnitudes are high- $z$  galaxies.

ment error from the stacked photometry, the candidate is eliminated. This procedure is performed in the band in which the source photometry has the highest signal-to-noise (S/N) ratio (typically the  $z$  band for  $i$  dropouts and the  $y$  band for  $z$  dropouts). We also reject candidates with too compact, diffuse, or elliptical profiles to be celestial point sources with the Source Extractor measurements on the stacked images. The eliminated sources are mostly cosmic rays, moving or transient sources, and image artifacts. Finally we inspect images of all the remaining candidates by eye, and reject additional problematic objects.

In the present survey area covering  $80 \text{ deg}^2$ , we had roughly 50,000 red point sources meeting the database query conditions (Equations 3 and 4) and undetected in the  $g$  and  $r$  bands. Although  $\sim 35,000$  candidates further passed the Bayesian selection ( $P_Q^B > 0.1$ ), the vast majority ( $> 99.5\%$ ) of them were eliminated by checking per-visit photometry and source morphology as above. After the final visual inspection, only 38 sources are found in the Main sample. On the other hand, we are still in the process of optimizing the Auxiliary selection so that a reasonable number of candidates are extracted. The remaining part of this paper focuses on the Main sample, for which the follow-up spectroscopy has been partially carried out (§4).

### 3.4. Recovery of known quasars

Figure 3 presents the Main sample selected above as the magnitude histogram. We found 36  $i$ -band dropouts as  $z \sim 6$  quasar candidates, and two  $z$ -band dropouts as  $z \sim 7$  quasar candidates. The magnitudes of the former objects range from  $z_{AB} = 21.8$  mag to the limiting magnitude of our selection,  $z_{AB} = 24.5$  mag, while the latter objects are fairly bright in the  $y$  band, 21.7 and 22.6 mag.

There are five high- $z$  quasars identified prior to our survey in the present area. They are summarized in Table

1. We found that all of them successfully pass our selection criteria and end up in the Main sample, as marked by the dark blue cells in Figure 3. The Bayesian quasar probability is  $P_Q^B = 1.000$  in all cases. The figure implies that the success rate of our quasar selection is quite high at the brightest magnitudes; for example, three of the four candidates at  $z < 22.5$  mag are indeed previously-discovered high- $z$  quasars. The five known quasars include CFHQS J0216–0455 with  $z = 24.22$  mag, which, as we discussed in §1, is the faintest high- $z$  quasar ever discovered.

Thus our candidate selection works quite efficiently at the brighter magnitudes. We now start to explore the remainder of the sample with new spectroscopic observations, as described in the next section.

## 4. SPECTROSCOPY

We carried out spectroscopic follow-up observations of the quasar candidates in the 2015 Fall and 2016 Spring semesters. One of the candidates was observed with the Optical System for Imaging and low-Intermediate-Resolution Integrated Spectroscopy (OSIRIS; Cepa et al. 2000) mounted on the Gran Telescopio Canarias (GTC) in 2015 September, which led to the first discovery of a high- $z$  quasar from our project. We also observed 19 candidates with the Faint Object Camera and Spectrograph (FOCAS; Kashikawa et al. 2002) mounted on Subaru in 2015 November and December, and identified 14 more quasars and galaxies. We further obtained additional exposures for a few of the above objects in 2016 February. The journal of these discovery observations is presented in Table 2. The details of the observations are described in the following sections.

### 4.1. GTC/OSIRIS

GTC is a 10.4-m telescope located at the Observatorio del Roque de los Muchachos in La Palma, Spain. Our program (GTC19-15B; Iwasawa et al.) was awarded 14.4 hours in the 2015B semester. We used OSIRIS with the R2500I grism and  $1''.0$ -wide longslit, which provides spectral coverage from  $\lambda_{\text{obs}} = 0.74$  to  $1.0 \mu\text{m}$  with a resolution  $R \sim 1500$ . The observations were carried out in queue mode on dark nights with excellent weather conditions and the seeing  $0''.7 - 1''.0$ .

The data were reduced using the Image Reduction and Analysis Facility (IRAF<sup>32</sup>). Bias correction, flat fielding with dome flats, sky subtraction, and 1d extraction were performed in the standard way. The wavelength was calibrated with reference to the arc lamp spectra. The flux calibration was tied to the white dwarf standard stars Ross 640 and G191-B2B observed on the same nights. We corrected for the slit loss by scaling the spectra to match the HSC  $z$ -band magnitudes.

One of the Main candidates was observed in this GTC run and identified to be a quasar at  $z = 6.10$ . Its spectrum is presented in §5. In addition, we observed five candidates selected from the older (S14B) version of the HSC-SSP data release. These five objects are no longer quasar candidates with the revised photometry in our

<sup>32</sup> IRAF is distributed by the National Optical Astronomy Observatory, which is operated by the Association of Universities for Research in Astronomy (AURA) under a cooperative agreement with the National Science Foundation.

TABLE 1  
KNOWN HIGH- $z$  QUASARS IN THE HSC-SSP S15A FOOTPRINT.

RA	Dec	$i_{AB}$ (mag)	$z_{AB}$ (mag)	$y_{AB}$ (mag)	Comment
02:10:13.19	-04:56:20.7	$26.96 \pm 0.42$	$22.34 \pm 0.01$	$22.39 \pm 0.04$	$z = 6.44$ ; Willott et al. (2010a)
02:16:27.79	-04:55:34.1	$27.61 \pm 0.69$	$24.20 \pm 0.07$	$25.81 \pm 0.68$	$z = 6.01$ ; Willott et al. (2009)
02:27:43.30	-06:05:30.3	$25.49 \pm 0.12$	$22.05 \pm 0.01$	$22.03 \pm 0.03$	$z = 6.20$ ; Willott et al. (2009)
22:19:17.22	+01:02:49.0	$27.78 \pm 0.80$	$23.43 \pm 0.04$	$23.29 \pm 0.07$	$z = 6.16$ ; Kashikawa et al. (2015)
22:28:43.52	+01:10:32.0	$24.01 \pm 0.02$	$22.40 \pm 0.01$	$22.47 \pm 0.02$	$z = 5.95$ ; Zeimann et al. (2011)

NOTE. — The coordinates (J2000.0) and magnitudes were measured with the HSC data. All the objects have the Bayesian quasar probability  $P_Q^B = 1.000$ .

TABLE 2  
JOURNAL OF DISCOVERY OBSERVATIONS.

Target	Date			
GTC/OSIRIS; 2015 September				
	Sep 13	Sep 14		
HSC J2216-0016	90 min	55 min		
Subaru/FOCAS; 2015 November and December				
	Nov 3	Nov 4	Dec 6	Dec 7
HSC J1205-0000	...	...	100 min <sup>s</sup>	...
HSC J2236+0032	25 min <sup>s</sup>	80 min	...	...
HSC J0859+0022	...	...	30 min	...
HSC J1152+0055	...	...	15 min	...
HSC J2232+0012	60 min	...	...	50 min <sup>e</sup>
HSC J2216-0016	...	...	...	30 min
HSC J2228+0128	80 min	...	...	...
HSC J1207-0005	...	...	...	40 min
HSC J1202-0057	...	...	...	60 min
HSC J0219-0416	80 min	...	...	60 min
HSC J0210-0523	23 min	...	60 min	...
HSC J0857+0142	...	...	...	100 min
HSC J0210-0559	80 min	...	45 min	...
HSC J0848+0045	80 min <sup>t</sup>	30 min <sup>s</sup>	30 min	...
HSC J0215-0555	...	40 min <sup>s,t</sup>	120 min	60 min
HSC J0850+0012	...	...	30 min	...
Subaru/FOCAS; 2016 February				
	Feb 13	Feb 14	Feb 15	Feb 16
HSC J1205-0000	...	...	80 min	100 min <sup>s</sup>
HSC J1207-0005	...	60 min	...	...
HSC J1202-0057	50 min	...	60 min	...
HSC J0210-0523	...	...	30 min <sup>e</sup>	40 min

NOTE. — Observing conditions: <sup>s</sup>poor seeing ( $1''.0 \sim 2''.0$ ), <sup>t</sup>low transparency, <sup>e</sup>low elevation ( $\sim 30$  deg).

fiducial (S15A) release, and hence are not included in the current Main sample. Indeed, their OSIRIS spectra show relatively smooth red continua characteristic of brown dwarfs, which are also consistent with the latest HSC magnitudes. The detailed analysis of these objects is still underway and will be reported in a future paper.

#### 4.2. Subaru/FOCAS

Our program was awarded four nights in the S15B semester (S15B-070; Matsuoka et al.) and five nights in the S16A semester (S16A-076; Matsuoka et al.) with the Subaru 8.2-m telescope. We used FOCAS in the multi-object spectrograph mode with the VPH900 grism and SO58 order-sorting filter. The widths of the slitlets were set to  $1''.0$ . This configuration provides spectral coverage from  $\lambda_{\text{obs}} = 0.75$  to  $1.05 \mu\text{m}$  with a resolution  $R \sim 1200$ . The observations were carried out in grey nights in 2015 November, December, and 2016 February. A few of these

nights were occasionally affected by cirrus and poor seeing ( $1''.0 \sim 2''.0$ ), while the weather was fairly good with seeing  $0''.6 - 0''.8$  in the rest of the observations.

The data were reduced with IRAF using the dedicated FOCASRED package. Bias correction, flat fielding with dome flats, sky subtraction, and 1d extraction were performed in the standard way. The wavelength was calibrated with reference to the sky emission lines. The flux calibration was tied to the white dwarf standard star Feige 110 observed on the same nights as the targets. We corrected for the slit loss by scaling the spectra to match the HSC magnitudes in the  $z$  band for the  $i$ -band dropouts and  $y$  band for the one  $z$ -band dropout we observed.

We observed 19 targets from the Main sample, including the quasar identified with GTC/OSIRIS, and identified 14 new high- $z$  quasars and galaxies as well as a brown dwarf. Their final spectra are presented in §5. One of the  $z$ -band dropout targets was not found at the HSC position at the time of the spectroscopy, so is most likely a moving object or a transient event caught by the HSC  $y$ -band observations. All the  $y$ -band exposures of this object were taken in a single day, and our inspection of per-visit images did not detect significant day-scale motion or flux variation. The spectral S/N of the remaining two targets is too low to judge their nature at this moment.

## 5. DISCOVERY OF HIGH- $Z$ QUASARS AND GALAXIES

Figure 4 displays the spectra of the identified quasars and possible quasars, while Figure 5 displays those of the non-quasars, i.e., galaxies and a brown dwarf. Their photometric and spectroscopic properties are summarized in Table 3. We first present short notes on the individual quasars in §5.1 and then on the contaminating objects in §5.2. Discussion and future prospects are described in §5.3.

### 5.1. Notes on individual quasars

#### 5.1.1. HSC J1205-0000

This object is a  $z$ -band dropout source with the HSC photometry. While the deep IGM absorption trough at  $\lambda_{\text{obs}} < 9350 \text{ \AA}$  suggests the redshift of this source is  $z \gtrsim 6.7$ , the interpretation of the redder part of the spectrum is difficult with the present S/N. If we assume that the strongest peak at  $\lambda_{\text{obs}} = 9550 \text{ \AA}$  is the Ly  $\alpha$  line, then the redshift is  $z = 6.85$ . In this case, the residual flux around  $9400 \text{ \AA}$  would imply that there is an ionized bubble at  $z \sim 6.7$  within the IGM, which might be caused by the quasar itself (e.g., Carilli et al. 2010) or a different source in front of the quasar. Alternatively, the Ly  $\alpha$  line may be at a shorter wavelength and significantly affected by



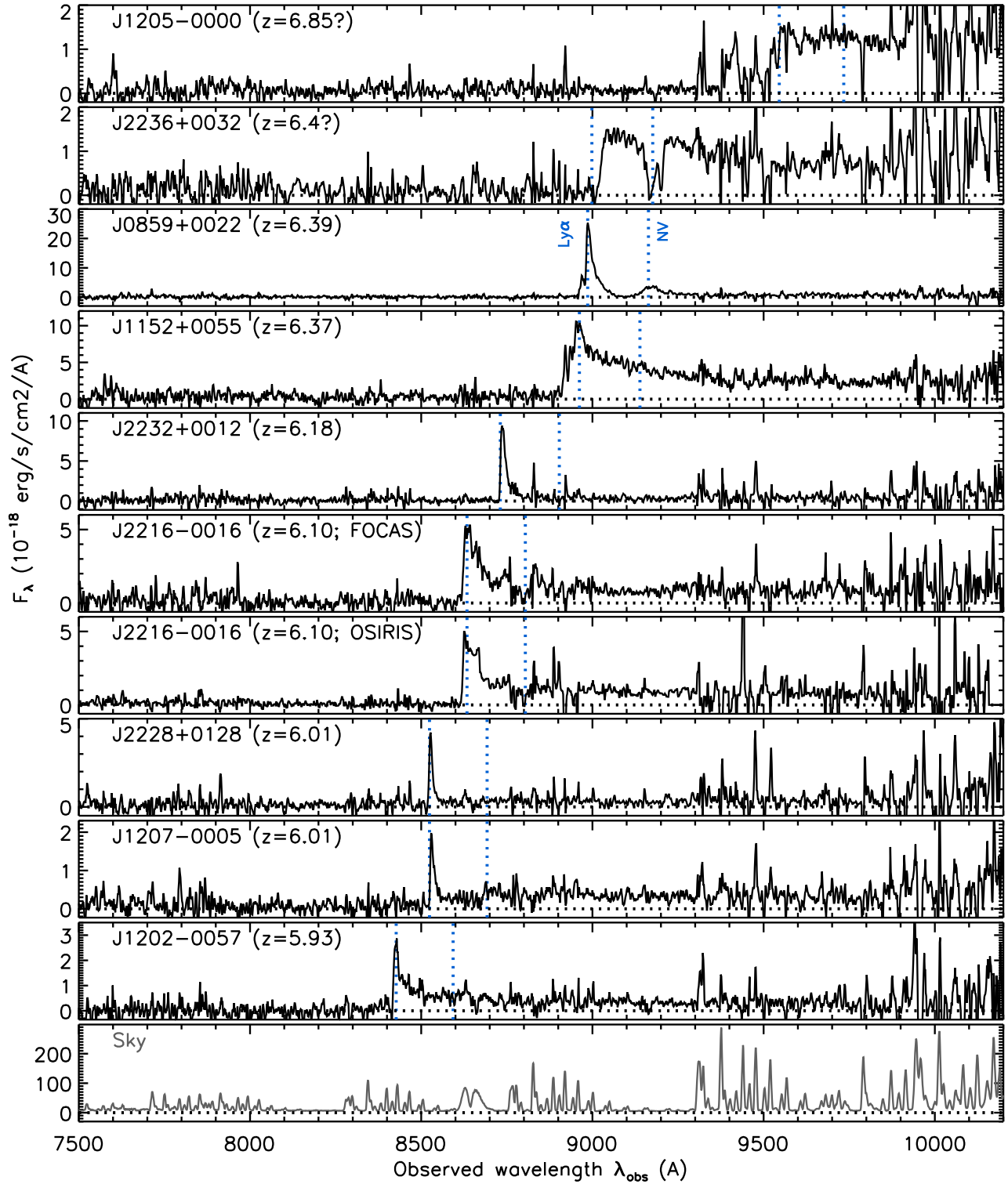


FIG. 4.— The reduced spectra of the quasars and possible quasars discovered in this work, displayed in decreasing order of redshift. The object name and the estimated redshift are indicated at the top left corner of each panel. The blue dotted lines mark the expected positions of the Ly  $\alpha$  and N V  $\lambda 1240$  emission lines. The spectra were smoothed using inverse-variance weighted means in 3 – 7 pixel (depending on the S/N) boxes, for display purpose. The bottom panel displays a sky spectrum.

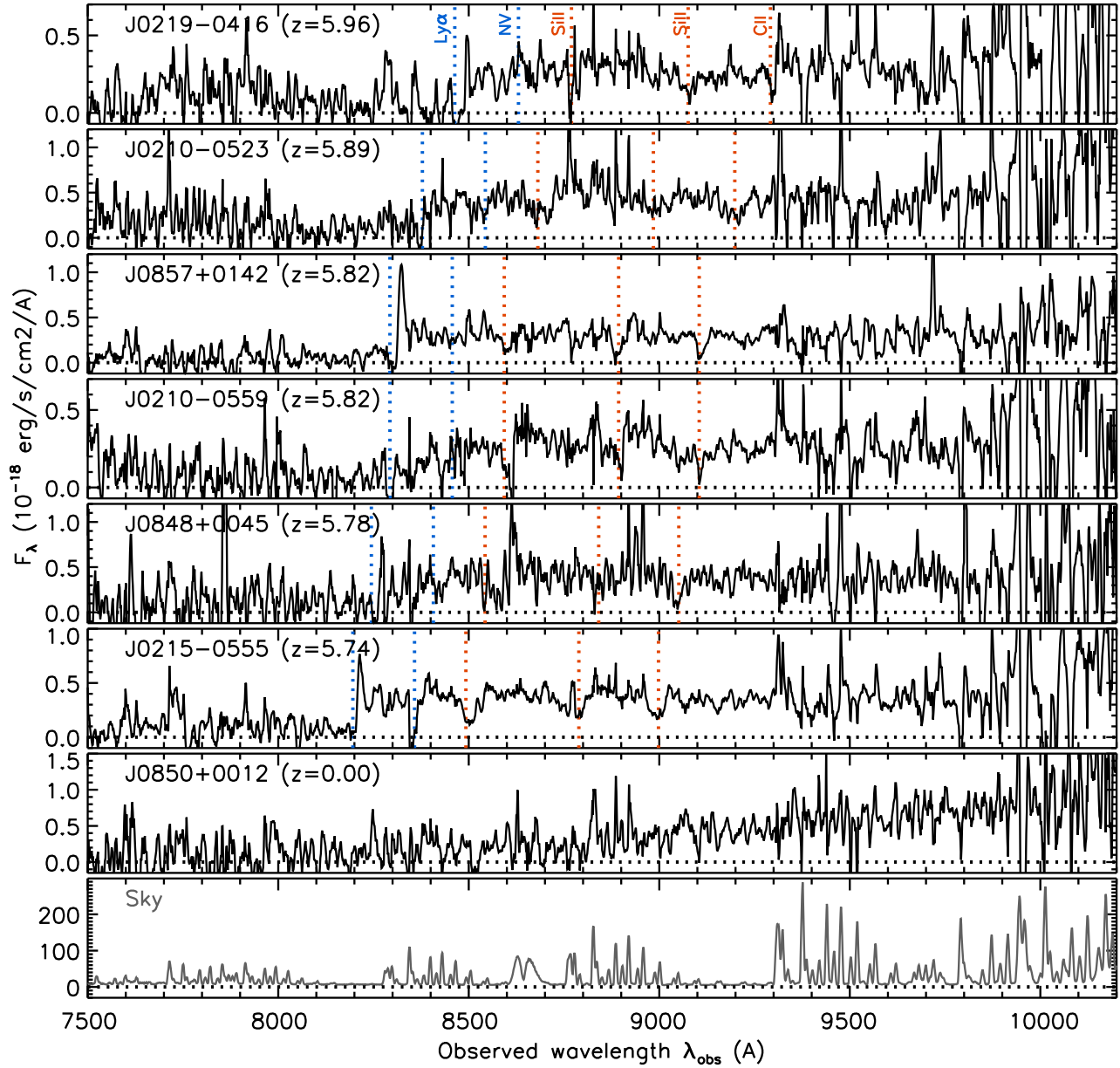


FIG. 5.— Same as Figure 4, but for the high- $z$  galaxies (top six panels) and the brown dwarf (J0850+0012). The expected positions of the interstellar absorption lines of Si II  $\lambda 1260$ , Si II  $\lambda 1304$ , and C II  $\lambda 1335$  are marked by the red dotted lines for the galaxies.

a broad absorption line (BAL) system of N V  $\lambda$ 1240. If the 9550 Å peak is assumed to be the N V line, then the estimated redshift is  $z = 6.70$  and Ly  $\alpha$  is at 9365 Å where no or little flux is observed.

#### 5.1.2. *HSC J2236+0032*

The IGM absorption trough at  $\lambda_{\text{obs}} < 9000$  Å indicates that the redshift of this source is  $z \gtrsim 6.4$ . The redder part of the spectrum is relatively blue and indicates this object is a quasar with no Ly  $\alpha$  emission line. The absence of Ly  $\alpha$  may be due to the intrinsic nature of this quasar or by the damping wing of severe IGM absorption. If we assume the Ly  $\alpha$  wavelength of  $\lambda_{\text{obs}} = 9000$  Å, then the estimated redshift is  $z = 6.4$ . In this case, the spectral position of the strong BAL observed at around 9200 Å corresponds to N V  $\lambda$ 1240. Indeed, quasars with weak or no Ly  $\alpha$  emission have been reported in the literature (e.g., Fan et al. 1999; Diamond-Stanic et al. 2009; Shemmer et al. 2010).

#### 5.1.3. *HSC J0859+0022*

This is an unambiguous quasar with strong and broad emission lines at  $\lambda_{\text{obs}} = 8990$  and 9170 Å, which are Ly  $\alpha$  and N V  $\lambda$ 1240 at  $z = 6.39$ . The continuum is very weak even at the wavelengths unaffected by IGM absorption (i.e., redwards of the Ly  $\alpha$  line), which may suggest the presence of significant dust extinction around the quasar nucleus or in the host galaxy.

#### 5.1.4. *HSC J1152+0055*

The spectrum is typical of a high- $z$  quasar. The redshift measured with the Ly  $\alpha$  line is  $z = 6.37$ , but is quite uncertain, given the asymmetry in the line due to the onset of the Ly  $\alpha$  forest.

#### 5.1.5. *HSC J2232+0012*

The spectrum is reminiscent of those of Ly  $\alpha$  emitters found in deep galaxy surveys (e.g., Ono et al. 2012). The Ly  $\alpha$  redshift is  $z = 6.18$ . The luminosity, rest-frame equivalent width, and full width at half maximum (FWHM; after correcting for the instrumental broadening) of the line are  $L(\text{Ly}\alpha) \sim 10^{43.9}$  erg s $^{-1}$ ,  $W_0(\text{Ly}\alpha) \sim 80$  Å, and  $v_{\text{FWHM}}(\text{Ly}\alpha) \sim 540$  km s $^{-1}$ , respectively. The high  $L(\text{Ly}\alpha)$  may imply the presence of AGN contribution, as a recent study of a large sample of Lyman  $\alpha$  emitters at  $z = 2.2$  (Konno et al. 2016) suggests that the bright emitters with  $L(\text{Ly}\alpha) > 10^{43.4}$  erg s $^{-1}$  are almost always contributed by AGNs, based on their X-ray, UV, or radio properties. The measured  $L(\text{Ly}\alpha)$  and  $v_{\text{FWHM}}(\text{Ly}\alpha)$  are similar to those of the high- $z$  galaxy ‘‘CR7’’ which is suggested to contain Population-III-like stars (Sobral et al. 2015, based on the very strong nebular lines including He II  $\lambda$ 1640), while  $W_0(\text{Ly}\alpha)$  is less than half that of CR7. The AGN contribution in this object may also be supported by the possible broad-line component seen at the redwards of Ly  $\alpha$ , as well as the relatively large  $v_{\text{FWHM}}(\text{Ly}\alpha)$  (see, e.g., Alexandroff et al. 2013). Note that the intrinsic line FWHM should be up to twice larger than estimated here, due to the IGM absorption.

#### 5.1.6. *HSC J2216–0016*

This is an unambiguous quasar at  $z = 6.10$ , observed both at GTC and Subaru. The spectrum around the expected N V  $\lambda$ 1240 position ( $\lambda_{\text{obs}} = 8790$  Å) is heavily absorbed, likely due to a BAL of the N V line. The small-scale features of this BAL are very similar in the FOCAS and OSIRIS spectra, suggesting they are real. We note that there is no atmospheric absorption features in the standard star spectrum corresponding to this BAL.

#### 5.1.7. *HSC J2228+0128*

The redshift measured with Ly  $\alpha$  is  $z = 6.01$ . The spectrum is similar to but not as extreme as J2232+0012, with  $L(\text{Ly}\alpha) \sim 10^{43.2}$  erg s $^{-1}$ ,  $W_0(\text{Ly}\alpha) \sim 20$  Å, and  $v_{\text{FWHM}}(\text{Ly}\alpha) \sim 250$  km s $^{-1}$ . As in J2232+0012, the luminous Ly  $\alpha$  line may be contributed in part by an AGN.

#### 5.1.8. *HSC J1207–0005*

The spectrum is very similar to that of the previous object, J2228+0128. The redshift inferred from the Ly  $\alpha$  line is  $z = 6.01$ , while the Ly  $\alpha$  properties are  $L(\text{Ly}\alpha) \sim 10^{42.9}$  erg s $^{-1}$ ,  $W_0(\text{Ly}\alpha) \sim 10$  Å, and  $v_{\text{FWHM}}(\text{Ly}\alpha) \sim 410$  km s $^{-1}$ . While the Ly  $\alpha$  emission is weaker than those in J2232+0012 and J2228+0128, the relatively large  $v_{\text{FWHM}}(\text{Ly}\alpha)$  may hint at the presence of AGN contribution.

#### 5.1.9. *HSC J1202–0057*

This object has a typical quasar spectrum, with strong and broad Ly  $\alpha$  line and blue continuum. The redshift estimated with Ly  $\alpha$  is  $z = 5.93$ .

### 5.2. *Notes on the contaminating objects*

Figure 5 presents the reduced spectra of the objects which are not likely to be quasars, based on the absence of high ionization lines, broad emission lines, or blue continuum. J0857+0142 and J0215–0555 have narrow Ly  $\alpha$  lines and sharp continuum breaks characteristic of GP troughs. The interstellar absorption lines of Si II  $\lambda$ 1260, Si II  $\lambda$ 1304, and C II  $\lambda$ 1335 are also clearly visible, which indicate that they are LBGs at  $z = 5.89$  and  $z = 5.74$ , respectively. These three absorption lines may also be present in the spectra of J0219–0416, J0210–0523, J0210–0559, and J0848+0045, although the S/N is lower. Combined with the relatively flat continua and the sharp flux drops in the bluer part of the spectra, they are likely to be high- $z$  galaxies as well. Their approximate redshifts were estimated from the absorption lines. The strong absorption lines created by the low-ionization species may be useful to estimate the escape fraction of ionizing photons in these galaxies (Jones et al. 2013), which will be addressed in future work.

It is worth noting that the redshift distribution of these contaminating galaxies ( $5.7 < z < 6.0$ ) is systematically different from that of the discovered quasars ( $5.9 < z < 6.9$ ). This is at least partly because only intrinsically luminous objects can be detected at  $z > 6.0$ , where the GP trough comes into the  $z$  band. It may also reflect the evolution of the luminous end of the galaxy luminosity function around  $z \sim 6$ .

Finally, J0850+0012 has a relatively smooth red continuum characteristic of a brown dwarf. Indeed this object has a rather low  $P_Q^B$  value ( $P_Q^B = 0.17$ ) and the Bayesian algorithm predicts it is most likely a L0 dwarf, which is consistent with the obtained spectrum. Follow-up study of this faint dwarf will be presented in a future paper.

### 5.3. Discussion and future prospects

In summary, we observed 19 out of the 38 Main candidates and identified 15 new high- $z$  quasars and galaxies. The above candidates also include 5 previously-known quasars, recovered by our selection. The current status of the spectroscopic identifications is presented in Figure 3. Our selection is quite successful at magnitudes brighter than  $z_{AB} = 23.5$  mag, where seven out of the nine candidates have turned out to be quasars and the remaining two are awaiting spectroscopy. This implies the following two points. First, the source detection and measurements with the HSC hardware and reduction software are highly reliable without serious systematic effects. Second, our quasar selection algorithms work quite efficiently as long as they are fed with correct photometry information.

Interestingly, we have started to find high- $z$  galaxies as significant contaminants at  $z_{AB} > 23.5$  mag. This is not surprising, since the luminosity functions of quasars and LBGs are likely to intersect at  $\sim 24$  mag, with LBGs outnumbering quasars at fainter magnitudes (see Figure 2 and the discussion in §3). Figure 6 presents the difference between the PSF and cModel magnitudes, as a measure of source extendedness, for all the identified objects in this work. We found that most of the objects are consistent with being point sources ( $m_{PSF} - m_{cModel} \simeq 0$ ), while the three objects, including the possible quasar J2232+0012, appear to be extended. Since the host galaxy contribution is not always negligible for low-luminosity quasars we are looking for, as we previously mentioned, no clear cut can be defined to separate quasars and galaxies on this plane.

Meanwhile, the discovered galaxies are an important probe of the reionization era. For example, stellar populations in such high- $z$  bright galaxies can be studied in detail with high-quality spectra. Measurements of the interstellar absorption lines such as those observed in J0857+0142 and J0215-0555 have the potential to constrain the escape fraction of ionizing photons as we previously mentioned. Follow-up observations with facilities at other wavelengths, e.g., the Atacama Large Millimeter/submillimeter Array (ALMA), would also be useful to understand the nature of these galaxies in the high- $z$  Universe.

At the faintest magnitudes of our survey ( $24.0 < z_{AB} < 24.5$  mag), the photometric selection and spectroscopic identification become more challenging. Along with the increasing fraction of galaxies, we found a contaminating brown dwarf, which is expected from its low Bayesian quasar probability ( $P_Q^B = 0.17$ ; see §5.2). We were not able to confirm the nature of two candidates due to their low spectral S/N, although we typically spent a few hours per object with Subaru. They seem to have no strong emission lines and so may be galaxies or brown dwarfs, but no- or weak-line quasars such as J2236+0032 do ex-

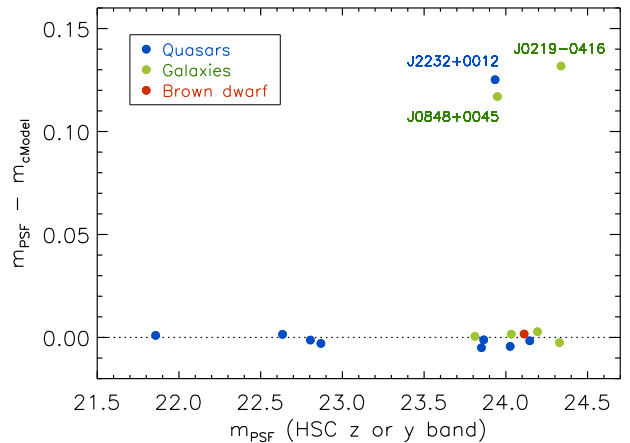


FIG. 6.— The difference between the PSF magnitude ( $m_{PSF}$ ) and cModel magnitude ( $m_{cModel}$ ) as a function of  $m_{PSF}$ , for quasars and possible quasars (blue), galaxies (green), and a brown dwarf (red). The magnitudes are measured in the  $y$  band for the  $z \sim 6.8$  quasar, J1205-0000, and in the  $z$  band for the remaining objects. Most of the objects are consistent with being point sources (around  $m_{PSF} - m_{cModel} = 0$ ; marked by the dotted line), while the three objects labelled with their names, including the possible quasar J2232+0012, appear to be extended.

ist. Further analysis of these objects, possibly with additional observing time to increase the S/N, will be presented in a future paper.

With the five previously-known objects and the nine objects (including the possible quasars J2232+0012, J2228+0128, and J1207-0005) newly identified, 14 high- $z$  quasars are now known in the present survey area. This is roughly half of the expected number with our survey limit in  $80 \text{ deg}^2$  (see §2), although the spectroscopic identification is still not complete. In the last column of Table 3, we report the absolute magnitudes of the discovered quasars as well as galaxies. For quasars, we measure the flux densities at the rest-frame wavelength  $\lambda_{rest} = 1270 - 1330 \text{ \AA}$  (except for J1205-0000 with the highest redshift, in which case we adopt  $\lambda_{rest} = 1250 - 1260 \text{ \AA}$ ) and estimate  $M_{1450}$  assuming the power-law continuum slope  $\alpha = -1.5$  ( $f_\lambda \propto \lambda^\alpha$ ; e.g., Vanden Berk et al. 2001). For galaxies, we directly measure  $M_{1350}$  at  $\lambda_{rest} = 1320 - 1380 \text{ \AA}$ . As expected, our survey has succeeded in identifying quasars (and galaxies) with luminosities approaching  $M_{1450} \sim -22$  mag, i.e.,  $\sim 2$  mag lower luminosity than found in most of the previous large surveys (see §1).

One important application of the discovered quasars is to measure the IGM H I opacity, and thus the progress of reionization, through the GP troughs. We checked the feasibility of this application by measuring inverse-variance weighted means of the residual flux in the obtained spectra, in bins of  $100 \text{ \AA}$  from  $\lambda_{obs} = 8000 \text{ \AA}$  to  $\sim 100 \text{ \AA}$  bluewards of Ly  $\alpha$ . There are 68 bins in total for all the quasars, in which (46, 28, 11) bins have more than ( $1\sigma$ ,  $2\sigma$ ,  $3\sigma$ ) flux detection. This suggests that these sources are potentially suited for IGM opacity measurements, which will be a subject of future work. Note that high S/N is crucial for robust GP measurements (White et al. 2003), which will require much longer integration time than we spent in the discovery observations for these sources.

We will continue and develop the SHELLQs project as

the HSC-SSP survey continues. The present work only partially covers the first  $80 \text{ deg}^2$  of the Wide layer, which will eventually observe  $1,400 \text{ deg}^2$ . Our immediate goal is to complete the spectroscopic identification in this  $80 \text{ deg}^2$  area and derive our first quasar luminosity function. In the long term, we will expand the survey area and significantly increase the sample size and luminosity range of known high- $z$  quasars. As described in §1, the expected numbers of quasars over the whole Wide area are  $\sim 500$  with  $z_{\text{AB}} < 24.5 \text{ mag}$  at  $z \sim 6$  and  $\sim 100$  with  $y_{\text{AB}} < 24.0 \text{ mag}$  at  $z \sim 7$ . We will also explore even lower luminosities with the Deep and Ultra-Deep layers of the HSC-SSP survey, though follow-up spectroscopy will become more challenging.

At the same time, it is important to follow up individual quasars in greater detail. The redshifts of some of the discovered quasars are poorly constrained at the moment, which should be improved. We are also preparing for deep optical and NIR spectroscopy to measure the near-zone size, SMBH mass, and metallicity for those quasars at lower luminosity than previously known at  $z > 6$ . These low-luminosity objects are expected to be much more numerous than the brighter ones, and hence possess critical information about the general properties of quasars in the early Universe. They will also provide a useful constraint on the low mass end of the SMBH mass function, and in turn models of the formation and early evolution of SMBHs. In addition, X-ray observations will play a critical role to estimate the bolometric luminosity, the Eddington ratio, and the presence and properties of absorbing material. We also plan to conduct ALMA follow-up observations in order to study the gas and dust content as well as the star formation activity in the host galaxies.

## 6. SUMMARY

We present initial results from the SHELLQs project, a survey of low-luminosity quasars and AGNs at high redshift close to the reionization era. The project exploits the exquisite imaging data with five optical bands ( $g$ ,  $r$ ,  $i$ ,  $z$ ,  $y$ ) produced by the Subaru HSC-SSP survey, supplemented with NIR photometry where available from UKIDSS and VIKING. The limiting magnitudes of the quasar search are currently set to  $z_{\text{AB}} < 24.5 \text{ mag}$  and  $y_{\text{AB}} < 24.0 \text{ mag}$ , but these may change in the future. The candidates are selected by combining several photometric approaches including a Bayesian probabilistic algorithm, which have turned out to be quite efficient in eliminating astrophysical contaminants such as stars and dwarfs, as well as cosmic rays, moving objects, and transient events. From the early HSC-SSP survey area covering  $80 \text{ deg}^2$ , we identified 38 candidates of high- $z$  quasars, which are the focus of this paper.

We carried out spectroscopic follow-up observations of 19 of these candidates, with GTC/OSIRIS and Subaru/FOCAS, in the 2015 Fall and 2016 Spring semesters. Nine objects were identified as quasars or possible quasars at  $5.9 < z < 6.9$ , based on the sharp continuum breaks characteristic of GP troughs, broad Ly $\alpha$  and N V  $\lambda 1240$  lines and/or blue continuum. Six objects are likely high- $z$  galaxies with interstellar absorption lines of Si II  $\lambda 1260$ , Si II  $\lambda 1304$ , and C II  $\lambda 1335$ , and in some cases narrow Ly $\alpha$  emission lines. The remaining objects include a L0 dwarf, a moving or transient object, and

two sources whose nature is still uncertain due to the low spectral S/N. In addition to these newly identified objects, there are five quasars known prior to our survey among the 38 candidates. The success rate of our selection is quite high, with most of the objects we took spectra of being identified as high- $z$  quasars or galaxies.

The SHELLQs project will continue as the HSC-SSP survey continues toward its goals of observing  $1400 \text{ deg}^2$  in the Wide layer, as well as  $27$  and  $3.5 \text{ deg}^2$  in the Deep and Ultra-Deep layer, respectively. We will soon deliver our first quasar luminosity function reaching down to  $M_{\text{AB}} \sim -22 \text{ mag}$  at  $z \sim 6$ . Further follow-up observations of the discovered quasars and galaxies are being considered at various wavelengths from sub-millimeter/radio to X-ray.

We are grateful to everyone involved in the hardware development, observations, and data reduction for the HSC-SSP survey. We had a lot of great help from Chien-Hsiu Lee, Takashi Hattori, and other Subaru staffs for the FOCAS observations. KI acknowledges support by the Spanish MINECO under grant AYA2013-47447-C3-2-P and MDM-2014-0369 of ICCUB (Unidad de Excelencia ‘María de Maeztu’). TN acknowledges financial support from the Japan Society for the Promotion of Science (KAKENHI grant no. 25707010) and also from the JGC-S Scholarship Foundation.

The Hyper Suprime-Cam (HSC) collaboration includes the astronomical communities of Japan and Taiwan, and Princeton University. The HSC hardware and instrumentation was built by the National Astronomical Observatory of Japan (NAOJ), the Kavli Institute for the Physics and Mathematics of the Universe (Kavli IPMU), the University of Tokyo, the High Energy Accelerator Research Organization (KEK), the Academia Sinica Institute for Astronomy and Astrophysics in Taiwan (ASIAA), and the Canon, Mitsubishi, and Hamamatsu Corporations. Funding was contributed by the Ministry of Education, Culture, Sports, Science and Technology (MEXT), the Japan Society for the Promotion of Science (JSPS), NAOJ, Kavli IPMU, KEK, ASIAA, and Princeton University.

*Facilities:* Subaru, GTC.

TABLE 3  
SPECTROSCOPICALLY-IDENTIFIED OBJECTS

Name	R.A.	Decl.	$i_{AB}$ (mag)	$z_{AB}$ (mag)	$y_{AB}$ (mag)	$J_{AB}$ (mag)	$P_Q^B$	$z$	$M_{1450/1350}^a$
quasars and possible quasars									
HSC J1205-0000	12:05:05.09	-00:00:27.9	> 26.69	> 26.45	$22.61 \pm 0.03$	$21.95 \pm 0.21$	1.000	6.85?	$-24.19 \pm 0.18$
HSC J2236+0032	22:36:44.58	+00:32:56.9	> 27.05	$23.78 \pm 0.08$	$23.23 \pm 0.05$	...	1.000	6.4?	$-23.55 \pm 0.44$
HSC J0859+0022	08:59:07.19	+00:22:55.9	$27.89 \pm 1.06$	$22.77 \pm 0.01$	$23.65 \pm 0.07$	> 21.77	1.000	6.39	$-23.56 \pm 0.15$
HSC J1152+0055	11:52:21.27	+00:55:36.6	$25.52 \pm 0.09$	$21.83 \pm 0.01$	$21.61 \pm 0.02$	$21.66 \pm 0.22$	1.000	6.37	$-24.91 \pm 0.12$
HSC J2232+0012	22:32:12.03	+00:12:38.4	$27.76 \pm 0.51$	$23.84 \pm 0.04$	$24.26 \pm 0.13$	...	1.000	6.18	$-22.70 \pm 0.40$
HSC J2216-0016	22:16:44.47	-00:16:50.1	$26.05 \pm 0.14$	$22.78 \pm 0.02$	$22.94 \pm 0.03$	...	1.000	6.10	$-23.56 \pm 0.13$
HSC J2228+0128	22:28:27.83	+01:28:09.5	$27.56 \pm 0.41$	$24.06 \pm 0.05$	$24.50 \pm 0.13$	...	1.000	6.01	$-22.36 \pm 0.11$
HSC J1207-0005	12:07:54.14	-00:05:53.3	$26.39 \pm 0.15$	$24.00 \pm 0.03$	$23.87 \pm 0.08$	> 21.77	1.000	6.01	$-22.57 \pm 0.08$
HSC J1202-0057	12:02:46.37	-00:57:01.7	$26.13 \pm 0.13$	$23.82 \pm 0.03$	$23.89 \pm 0.10$	> 21.77	1.000	5.93	$-22.44 \pm 0.35$
galaxies									
HSC J0219-0416	02:19:29.41	-04:16:45.9	> 26.74	$24.32 \pm 0.06$	$24.14 \pm 0.11$	> 21.78	1.000	5.96	$-22.53 \pm 0.14$
HSC J0210-0523	02:10:33.82	-05:23:04.1	$25.85 \pm 0.17$	$23.78 \pm 0.06$	$23.54 \pm 0.11$	...	0.940	5.89	$-22.89 \pm 0.23$
HSC J0857+0142	08:57:23.95	+01:42:54.6	$26.24 \pm 0.26$	$24.14 \pm 0.05$	$23.93 \pm 0.09$	> 21.76	0.964	5.82	$-22.48 \pm 0.03$
HSC J0210-0559	02:10:41.28	-05:59:17.9	$26.61 \pm 0.27$	$24.25 \pm 0.07$	$24.10 \pm 0.16$	...	0.996	5.82	$-22.31 \pm 0.12$
HSC J0848+0045	08:48:18.33	+00:45:09.6	$26.27 \pm 0.21$	$23.90 \pm 0.06$	$24.00 \pm 0.10$	> 21.76	1.000	5.78	$-22.75 \pm 0.61$
HSC J0215-0555	02:15:45.20	-05:55:29.1	$26.03 \pm 0.15$	$23.98 \pm 0.05$	$23.67 \pm 0.10$	...	0.929	5.74	$-22.65 \pm 0.24$
brown dwarf									
HSC J0850+0012	08:50:02.63	+00:12:10.0	$28.40 \pm 1.44$	$24.06 \pm 0.06$	$23.22 \pm 0.05$	> 21.76	0.171	0.00	...

NOTE. — The coordinates are at J2000.0. The magnitude upper limits are placed at  $5\sigma$  significance.

<sup>a</sup> Absolute magnitudes measured at the rest-frame wavelength  $\lambda_{\text{rest}} = 1450 \text{ \AA}$  ( $M_{1450}$ ) for quasars and at  $\lambda_{\text{rest}} = 1350 \text{ \AA}$  ( $M_{1350}$ ) for galaxies.



## REFERENCES

- Abazajian, K., Adelman-McCarthy, J. K., Agüeros, M. A., et al. 2004, *AJ*, 128, 502
- Alexandroff, R., Strauss, M. A., Greene, J. E., et al. 2013, *MNRAS*, 435, 3306
- Bañados, E., Venemans, B. P., Morganson, E., et al. 2014, *AJ*, 148, 14
- Bertin, E., & Arnouts, S. 1996, *A&AS*, 117, 393
- Bouwens, R. J., Illingworth, G. D., Blakeslee, J. P., & Franx, M. 2006, *ApJ*, 653, 53
- Bouwens, R. J., Illingworth, G. D., Oesch, P. A., et al. 2015, *ApJ*, 803, 34
- Bouwens, R. J., Illingworth, G. D., Oesch, P. A., et al. 2011, *ApJ*, 737, 90
- Carnall, A. C., Shanks, T., Chehade, B., et al. 2015, *MNRAS*, 451, L16
- Caballero, J. A., Burgasser, A. J., & Klement, R. 2008, *A&A*, 488, 181
- Carilli, C. L., Wang, R., Fan, X., et al. 2010, *ApJ*, 714, 834
- Cepa, J., Aguiar, M., Escalera, V. G., et al. 2000, *Proc. SPIE*, 4008, 623
- Choudhury, T. R., Puchwein, E., Haehnelt, M. G., & Bolton, J. S. 2015, *MNRAS*, 452, 261
- Dark Energy Survey Collaboration, Abbott, T., Abdalla, F. B., et al. 2016, arXiv:1601.00329
- De Rosa, G., Decarli, R., Walter, F., et al. 2011, *ApJ*, 739, 56
- De Rosa, G., Venemans, B. P., Decarli, R., et al. 2014, *ApJ*, 790, 145
- Diamond-Stanic, A. M., Fan, X., Brandt, W. N., et al. 2009, *ApJ*, 699, 782
- Fan, X., Carilli, C. L., & Keating, B. 2006, *ARA&A*, 44, 415
- Fan, X., Hennawi, J. F., Richards, G. T., et al. 2004, *AJ*, 128, 515
- Fan, X., Narayanan, V. K., Lupton, R. H., et al. 2001, *AJ*, 122, 2833
- Fan, X., Strauss, M. A., Gunn, J. E., et al. 1999, *ApJ*, 526, L57
- Fan, X., Strauss, M. A., Richards, G. T., et al. 2001, *AJ*, 121, 31
- Fan, X., Strauss, M. A., Richards, G. T., et al. 2006, *AJ*, 131, 1203
- Fan, X., Strauss, M. A., Schneider, D. P., et al. 2003, *AJ*, 125, 1649
- Fan, X., White, R. L., Davis, M., et al. 2000, *AJ*, 120, 1167
- Ferrara, A., Salvadori, S., Yue, B., & Schleicher, D. 2014, *MNRAS*, 443, 2410
- Fontanot, F., Cristiani, S., & Vanzella, E. 2012, *MNRAS*, 425, 1413
- Fukugita, M., Ichikawa, T., Gunn, J. E., et al. 1996, *AJ*, 111, 1748
- Furusawa, H., Kosugi, G., Akiyama, M., et al. 2008, *ApJS*, 176, 1
- Giallongo, E., Grazian, A., Fiore, F., et al. 2015, *A&A*, 578, A83
- González, V., Bouwens, R. J., Labbé, I., et al. 2012, *ApJ*, 755, 148
- Goto, T. 2006, *MNRAS*, 371, 769
- Goto, T., Utsumi, Y., Furusawa, H., Miyazaki, S., & Komiyama, Y. 2009, *MNRAS*, 400, 843
- Goto, T., Utsumi, Y., Walsh, J. R., et al. 2012, *MNRAS*, 421, L77
- Grissom, R. L., Ballantyne, D. R., & Wise, J. H. 2014, *A&A*, 561, A90
- Gunn, J. E., & Peterson, B. A. 1965, *ApJ*, 142, 1633
- Hewett, P. C., Warren, S. J., Leggett, S. K., & Hodgkin, S. T. 2006, *MNRAS*, 367, 454
- Jee, M. J., & Tyson, J. A. 2011, *PASP*, 123, 596
- Jiang, L., Fan, X., Annis, J., et al. 2008, *AJ*, 135, 1057
- Jiang, L., Fan, X., Bian, F., et al. 2009, *AJ*, 138, 305
- Jiang, L., McGreer, I. D., Fan, X., et al. 2015, *AJ*, 149, 188
- Jiang, L., Fan, X., Vestergaard, M., et al. 2007, *AJ*, 134, 1150
- Jones, T. A., Ellis, R. S., Schenker, M. A., & Stark, D. P. 2013, *ApJ*, 779, 52
- Jurić, M., Kantor, J., Lim, K., et al. 2015, arXiv:1512.07914
- Kashikawa, N., Aoki, K., Asai, R., et al. 2002, *PASJ*, 54, 819
- Kashikawa, N., Ishizaki, Y., Willott, C. J., et al. 2015, *ApJ*, 798, 28
- Kashikawa, N., Kitayama, T., Doi, M., et al. 2007, *ApJ*, 663, 765
- Kaiser, N., Aussel, H., Burke, B. E., et al. 2002, *Proc. SPIE*, 4836, 154
- Kaiser, N., Burgett, W., Chambers, K., et al. 2010, *Proc. SPIE*, 7733, 77330E
- Kawaguchi, T., Aoki, K., Ohta, K., & Collin, S. 2004, *A&A*, 420, L23
- Kim, Y., Im, M., Jeon, Y., et al. 2015, *ApJ*, 813, L35
- Konno, A., Ouchi, M., Nakajima, K., et al. 2015, arXiv:1512.01854
- Konno, A., Ouchi, M., Ono, Y., et al. 2014, *ApJ*, 797, 16
- Lawrence, A., Warren, S. J., Almaini, O., et al. 2007, *MNRAS*, 379, 1599
- Lehnert, M. D., & Bremer, M. 2003, *ApJ*, 593, 630
- Madau, P., & Haardt, F. 2015, *ApJ*, 813, L8
- Madau, P., Haardt, F., & Dotti, M. 2014, *ApJ*, 784, L38
- Magnier, E. A., Schlafly, E., Finkbeiner, D., et al. 2013, *ApJS*, 205, 20
- Maiolino, R., Cox, P., Caselli, P., et al. 2005, *A&A*, 440, L51
- McGreer, I. D., Becker, R. H., Helfand, D. J., & White, R. L. 2006, *ApJ*, 652, 157
- Miyazaki, S., Komiyama, Y., Nakaya, H., et al. 2012, *Proc. SPIE*, 8446, 84460Z
- Mortlock, D. J., Patel, M., Warren, S. J., et al. 2012, *MNRAS*, 419, 390
- Mortlock, D. J., Warren, S. J., Venemans, B. P., et al. 2011, *Nature*, 474, 616
- Oke, J. B., & Gunn, J. E. 1983, *ApJ*, 266, 713
- Ono, Y., Ouchi, M., Mobasher, B., et al. 2012, *ApJ*, 744, 83
- Ouchi, M., Shimasaku, K., Akiyama, M., et al. 2008, *ApJS*, 176, 301
- Ouchi, M., Shimasaku, K., Furusawa, H., et al. 2010, *ApJ*, 723, 869
- Planck Collaboration, Ade, P. A. R., Aghanim, N., et al. 2015, arXiv:1502.01589
- Pickles, A. J. 1998, *PASP*, 110, 863
- Prevot, M. L., Lequeux, J., Prevot, L., Maurice, E., & Rocca-Volmerange, B. 1984, *A&A*, 132, 389
- Reed, S. L., McMahon, R. G., Banerji, M., et al. 2015, *MNRAS*, 454, 3952
- Richards, G. T., Fan, X., Newberg, H. J., et al. 2002, *AJ*, 123, 2945
- Robertson, B. E., Ellis, R. S., Dunlop, J. S., McLure, R. J., & Stark, D. P. 2010, *Nature*, 468, 49
- Robertson, B. E., Ellis, R. S., Furlanetto, S. R., & Dunlop, J. S. 2015, *ApJ*, 802, L19
- Robertson, B. E., Furlanetto, S. R., Schneider, E., et al. 2013, *ApJ*, 768, 71
- Schlafly, E. F., Finkbeiner, D. P., Jurić, M., et al. 2012, *ApJ*, 756, 158
- Schlegel, D. J., Finkbeiner, D. P., & Davis, M. 1998, *ApJ*, 500, 525
- Shapiro, S. L. 2005, *ApJ*, 620, 59
- Shemmer, O., Trakhtenbrot, B., Anderson, S. F., et al. 2010, *ApJ*, 722, L152
- Sobral, D., Matthee, J., Darvish, B., et al. 2015, *ApJ*, 808, 139
- Songaila, A. 2004, *AJ*, 127, 2598
- Tonry, J. L., Stubbs, C. W., Lykke, K. R., et al. 2012, *ApJ*, 750, 99
- Vanden Berk, D. E., Richards, G. T., Bauer, A., et al. 2001, *AJ*, 122, 549
- Venemans, B. P., Bañados, E., Decarli, R., et al. 2015, *ApJ*, 801, L11
- Venemans, B. P., Findlay, J. R., Sutherland, W. J., et al. 2013, *ApJ*, 779, 24
- Venemans, B. P., McMahon, R. G., Walter, F., et al. 2012, *ApJ*, 751, L25
- Venemans, B. P., Verdoes Kleijn, G. A., Mwebaze, J., et al. 2015, *MNRAS*, 453, 2259
- Venemans, B. P., Walter, F., Zschaechner, L., et al. 2016, *ApJ*, 816, 37
- Volonteri, M. 2012, *Science*, 337, 544
- Wang, R., Carilli, C. L., Beelen, A., et al. 2007, *AJ*, 134, 617
- Wang, R., Wagg, J., Carilli, C. L., et al. 2013, *ApJ*, 773, 44
- White, R. L., Becker, R. H., Fan, X., & Strauss, M. A. 2003, *AJ*, 126, 1
- Willott, C. J., Bergeron, J., & Omont, A. 2015, *ApJ*, 801, 123
- Willott, C. J., Chet, S., Bergeron, J., & Hutchings, J. B. 2011, *AJ*, 142, 186
- Willott, C. J., Delfosse, X., Forveille, T., Delorme, P., & Gwyn, S. D. J. 2005, *ApJ*, 633, 630
- Willott, C. J., Delorme, P., Omont, A., et al. 2007, *AJ*, 134, 2435

- Willott, C. J., Albert, L., Arzoumanian, D., et al. 2010a, *AJ*, 140, 546
- Willott, C. J., Delorme, P., Reylé, C., et al. 2010b, *AJ*, 139, 906
- Willott, C. J., Delorme, P., Reylé, C., et al. 2009, *AJ*, 137, 3541
- Willott, C. J., Omont, A., & Bergeron, J. 2013, *ApJ*, 770, 13
- Wu, X.-B., Wang, F., Fan, X., et al. 2015, *Nature*, 518, 512
- York, D. G., Adelman, J., Anderson, J. E., Jr., et al. 2000, *AJ*, 120, 1579
- Zeimann, G. R., White, R. L., Becker, R. H., et al. 2011, *ApJ*, 736, 57